

# Nuclear effects in prompt photon production at the Large Hadron Collider

J. Jalilian-Marian<sup>1,2</sup>, K. Orginos<sup>1,3</sup> and I. Sarcevic<sup>1</sup>

<sup>1</sup>*Department of Physics, University of Arizona, Tucson, Arizona 85721*

<sup>2</sup>*Physics Department, Brookhaven National Laboratory, Upton NY 11973-5000*

<sup>3</sup>*RIKEN-BNL Research Center, Brookhaven National Laboratory, Upton NY 11973-5000*

## Abstract

We present a detailed study of prompt photon production cross section in heavy-ion collisions in the central rapidity region at energy of  $\sqrt{s} = 5.5$  TeV, appropriate to LHC experiment. We include the next-to-leading order radiative corrections,  $O(\alpha_{em}\alpha_s^2)$ , nuclear shadowing and the parton energy loss effects. We find that the nuclear effects can reduce the invariant cross section for prompt photon production by an order of magnitude at  $p_t = 3$  GeV. We discuss theoretical uncertainties due to parton energy loss and nuclear shadowing parameters. We show that the K-factor, which signifies the importance of next-to-leading order corrections, is large and has a strong  $p_t$  dependence.

# 1 Introduction

There has been a considerable theoretical and experimental interest in studying photon production in heavy-ion collisions at BNL's Relativistic Heavy Ion Collider (RHIC) and CERN's Large Hadron Collider (LHC) energies [1]. Photons produced in heavy-ion collisions provide an excellent probe of the properties of the dense matter, such as the quark-gluon plasma or the hot hadronic gas, produced after the collision. Due to the small cross sections of electromagnetic interactions, photons can escape the strongly interacting matter produced in the collision without further interactions.

Studying photon production at the RHIC and LHC energies is of special interest, as it has been suggested as an elegant signal for detecting the formation of a quark-gluon plasma (QGP) in heavy-ion collisions [2]. However, photons can be produced at different stages of the heavy ion collision and thus have different origin. For example, photons can be produced at the early stages of the collision through QCD processes such as  $qg \rightarrow q\gamma$  or they can be emitted from a thermalized quark-gluon plasma or hadronic gas. Another source of produced photons is decay of hadrons such as pions and etas produced in the heavy ion collision [3]. Furthermore, different processes give the dominant contribution at different  $p_t$ 's. Therefore, it is quite difficult to make reliable predictions for the absolute number of photons produced in a heavy ion collision [4, 5].

Prompt photons are an important background to thermal photons in the low to intermediate  $p_t$  region and are dominant in the high  $p_t$  region. Therefore, it is extremely important to be able to calculate their production cross section reliably. Fortunately, one can use perturbative QCD in the high  $p_t$  region to calculate the prompt photon production cross section. In this work we continue our study of the production of high  $p_t$  ( $p_t > 3$  GeV) prompt photons in heavy ion collisions [6]. Prompt photons are produced either directly in the hard collisions of the partons inside the nuclei like  $qg \rightarrow q\gamma$  or through bremsstrahlung of quarks and gluons produced in the hard collision such as  $qg \rightarrow qq\gamma$ . We include all next-to-leading order,  $O(\alpha_{em}\alpha_s^2)$  QCD processes [7] as well as nuclear shadowing and medium induced parton energy loss effects. We discuss and estimate the theoretical uncertainties due to different choices of nuclear shadowing and energy loss parameters. We show that next-to-leading (NLO) corrections are large and must be included to make reliable predictions.

In section I we review the prompt photon production in hadronic collisions in next-to-leading order. Based on QCD factorization theorems, we write down the expression for prompt photon production and list the hard partonic processes involved. In section II we discuss the nuclear effects such as shadowing and energy loss involved in production of prompt photons in heavy ion collisions. In section III we present our results for the prompt photon production invariant cross section,  $E \frac{d\sigma}{d^3p}$ , at LHC energies and an estimate of the theoretical uncertainties due to variation of nuclear shadowing and energy loss parameters. We show that the effective K-factor, defined as the ratio of NLO to LO cross sections in heavy ion collisions is large and has a strong  $p_t$  dependence. This clearly shows the importance of including next-to-leading order contributions to prompt photon production. We conclude with a discussion of prospects for detecting nuclear effects by measuring

prompt photons at LHC.

## 2 Prompt photon production in pQCD

Using factorization theorems and perturbative QCD, the inclusive cross section for prompt photon production in a hadronic collision can be written as a convolution of parton densities in a hadron with the hard scattering cross section and the parton to photon fragmentation function:

$$E_\gamma \frac{d^3\sigma}{d^3p_\gamma}(\sqrt{s}, p_\gamma) = \int dx_a \int dx_b \int dz \sum_{i,j}^{partons} F_i(x_a, Q^2) F_j(x_b, Q^2) D_{c/\gamma}(z, Q_f^2) E_\gamma \frac{d^3\hat{\sigma}_{ij \rightarrow cX}}{d^3p_\gamma} \quad (1)$$

where the  $F_i(x, Q^2)$  is the  $i$ -th parton distribution in a nucleon,  $x_a$  and  $x_b$  are the fractional momenta of incoming partons,  $D_{c/\gamma}(z, Q_f^2)$  is the photon fragmentation function with  $z$  being the fraction of parton energy carried by the photon. The parton-parton cross sections,  $\frac{d^3\hat{\sigma}_{ij \rightarrow cX}}{d^3p_\gamma}$ , include all processes up to and including  $O(\alpha_{em}\alpha_s^2)$ , such as leading-order subprocesses:

$$\begin{aligned} q + \bar{q} &\rightarrow \gamma + g \\ q + g &\rightarrow \gamma + q \end{aligned} \quad (2)$$

and the next-to-leading order subprocesses,

$$\begin{aligned} q + q &\rightarrow q + q + \gamma \\ q + \bar{q} &\rightarrow q + \bar{q} + \gamma \\ q + q' &\rightarrow q + q' + \gamma \\ q + \bar{q} &\rightarrow q' + \bar{q}' + \gamma \\ q + \bar{q}' &\rightarrow q + \bar{q}' + \gamma \end{aligned} \quad (3)$$

We refer the reader to [7] for a complete list of all  $O(\alpha_{em}\alpha_s^2)$  processes. There are two classes of subprocesses, “direct” production, which does not have convolution with the fragmentation function and the “bremsstrahlung” contribution that has convolution with the fragmentation function. Direct subprocesses contribute to leading order as well as next-to-leading order, while bremsstrahlung processes only contribute at the next-to-leading order. Clearly, only the sum of these two contributions constitutes the full NLO calculation of the direct photon production. It is important to note that in order to include all  $O(\alpha_{em}\alpha_s^2)$  processes, it is necessary to include processes which formally look order  $O(\alpha_{em}\alpha_s^3)$ . This is because some of the terms in (3) have a divergence proportional to  $1/\alpha_s$  which makes those processes  $O(\alpha_{em}\alpha_s)$ . This divergence comes from the quark and emitted photon being collinear. The reader is referred to [8] for a discussion of the collinear divergences.

The nucleon structure functions,  $F_i(x, Q^2)$ , and parton to photon fragmentation functions,  $D_{c/\gamma}(z, Q_f^2)$ , are also evaluated at the next-to-leading order. We use the MRS99

set for nucleon structure functions [9] and Bourhis et al. parameterization of the photon fragmentation functions [10]. Structure functions, fragmentation functions and the running coupling constant depend on the factorization, fragmentation and renormalization scales respectively which are usually taken to be the same and proportional to the photon transverse momentum  $p_t$ . Aurenche et al. [11] have studied the dependence of the prompt photon cross section on the choice of scale and have shown that the choice of  $Q = p_t/2$  gives a very good description of prompt photon production in hadronic collisions. Therefore, we will use  $Q = p_t/2$  in our calculation. The running coupling constant  $\alpha_s(Q^2)$ , calculated to next-to-leading order, is given by

$$\alpha_s(Q^2) = \frac{12\pi}{(33 - 2N_f) \ln Q^2/\Lambda^2} \left[ 1 - \frac{6(153 - 19N_f) \ln \ln Q^2/\Lambda^2}{(33 - 2N_f)^2 \ln Q^2/\Lambda^2} \right] \quad (4)$$

where  $Q^2$  is the renormalization scale,  $\Lambda$  is the QCD scale parameter and  $N_f$  is the number of flavors.

In Figure (1a) we illustrate the importance of including the next-to-leading order contributions by calculating the ratio of NLO to LO cross sections, the so-called K-factor. Clearly, the NLO corrections are large and  $p_t$  dependent. It would be useful to go even beyond the NLO to make sure that the higher order corrections are not even larger. It is, however, clear that a leading order calculation in the LHC kinematic region is meaningless since the next-to-leading order corrections are huge.

In Figure (1b) we show an alternative definition of the K-factor defined as  $K \equiv NLO/(LO + Brems.)$  sometimes used in the literature [4]. The main reason for this definition was inclusion of an incomplete set of Bremsstrahlung diagrams in previous works on prompt photon cross sections [4] and we show it here for comparison.

In principle, in the region where  $x_t \sim p_t/\sqrt{s}$  is large, i.e. in the very low and very high  $p_t$  region of phase space, one would need to resum certain logarithmic terms, of the form  $\alpha_s \ln(1 - x_t)$  and  $\alpha_s \ln x_t$ . However, these resummations are not very important for the range of  $p_t$  and  $\sqrt{s}$  that are considered in this work and will be neglected [12].

There is also an alternative approach to calculating prompt photon cross sections which uses the LO cross sections as well as LO structure and fragmentation functions. In order to reproduce the experimental data in this approach, it is necessary to include a phenomenological parameter which is loosely identified as the ‘‘intrinsic’’ momentum of the initial state partons [13]. This intrinsic momentum is generated by the initial state radiation of quarks and gluons. There is however no theoretical calculation of these effects at the moment and one has to model them by generalizing the standard definitions of the parton distribution functions from  $q(x, Q^2)$  and  $G(x, Q^2)$  to  $q(x, k_t^2, Q^2)$  and  $G(x, k_t^2, Q^2)$ . One then introduces a weight function, typically a Gaussian, with a width  $\langle k_t^2 \rangle$  which represents the intrinsic transverse momentum of the initial state partons. Assuming some reasonable range in  $k_t$ , these intrinsic momenta are integrated over in the final result. This approach gives fairly good description of most of the experimental results.

It is important to realize that this intrinsic momentum  $k_t$  grows with energy and can be as large as  $\sim 1 - 2$  GeV in fixed target experiments and  $\sim 5$  GeV in the Tevatron [14]. Therefore, strictly speaking, it is not an intrinsic momentum. In addition, the value of  $k_t$  is

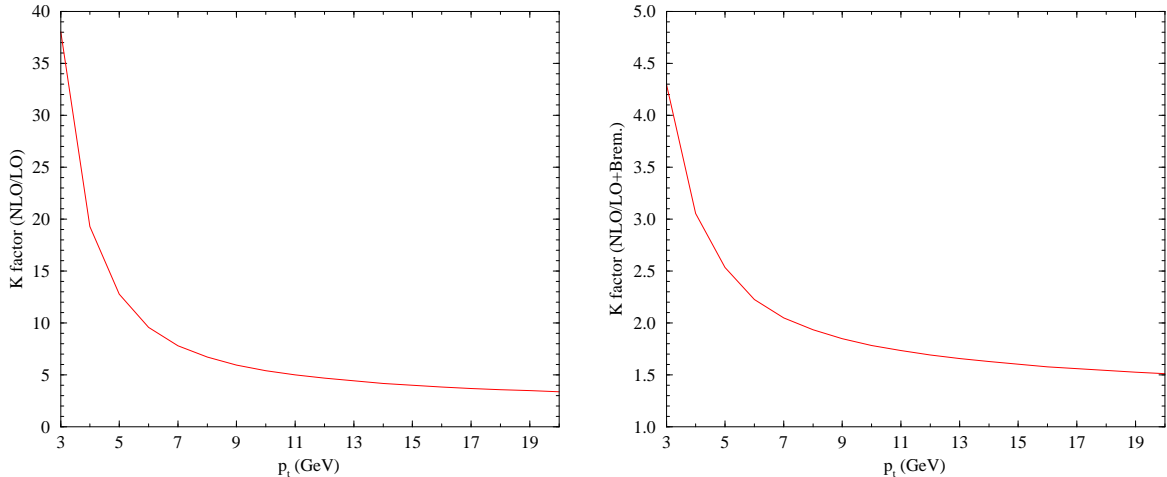


Figure 1: a) The hadronic K-factor defined as the ratio of NLO prompt photon cross section,  $E \frac{d\sigma}{d^3p}$  to the LO cross section, and b) the K-factor defined as the ratio of NLO to the LO plus bremsstrahlung cross sections.

process dependent and thus can not be taken as universal parameter. It might be possible to extract its value from the data in different experiments, but its value can not be predicted. In our work, we will not follow this approach but instead we will use NLO perturbative QCD formalism because it seems theoretically more rigorous and self-consistent. We note that NLO calculations give fairly good agreement with the experimental data for  $p_t > 3.5\text{GeV}$  at lower energies ( $\sqrt{s} \leq 63\text{ GeV}$ ) [11] and for  $p_t > 10\text{GeV}$  at higher energies ( $\sqrt{s} = 1800\text{ GeV}$ ) [14]. However, it is worth pointing out that there are claims of inconsistencies among various data sets from different experiments at low energies [11, 14]. In addition, one should keep in mind that our study extends down to lower values of  $p_t$ , where NLO predictions may not be reliable.

### 3 Prompt photon production in heavy ion collisions

To calculate the prompt photon production cross section in heavy ion collisions, we will use eq. (1) modified for nuclear effects:

$$E_\gamma \frac{d^3\sigma^{AB}}{d^3p_\gamma}(\sqrt{s}, p_t) = \int dx_a \int dx_b \int dz \sum_{i,j}^{partons} F_i^A(x_a, Q^2) F_j^B(x_b, Q^2) D_{c/\gamma}(z, Q_f^2) E_\gamma \frac{d^3\hat{\sigma}_{ij \rightarrow cX}}{d^3p_\gamma} \quad (5)$$

where the  $F_i^A(x, Q^2)$  is the  $i$ -th parton distribution in a nucleus and  $D_{c/\gamma}(z, Q_f^2)$  is the photon fragmentation function in a nuclear environment. The partonic processes (a partial list) are given by (2, 3) as before. The nuclear structure function  $F_i^A(x, Q^2)$  and fragmentation function  $D_{c/\gamma}(z, Q_f^2)$  are not known to next-to-leading order, but rather they are NLO

nucleon structure and fragmentation functions modified for nuclear effects. Strictly speaking, therefore, our calculation of prompt photon production in heavy ion collisions is not a next-to-leading order calculation but is the most complete calculation performed so far. Below, we will describe the nuclear modifications to structure functions and fragmentation functions in detail.

### 3.1 The Nuclear Shadowing Effect

Calculation of the prompt photons production cross section in nuclear collisions requires knowledge of the nuclear structure functions  $F_i^A(x, Q^2)$ , usually measured in Deep Inelastic Scattering (DIS) of electrons on nuclei. It is an experimental fact that  $F_i^A(x, Q^2) \neq AF_i^N(x, Q^2)$  where  $F_i^N(x, Q^2)$  is the free nucleon structure function. This modification has a strong  $x$  dependence and is due to having different nuclear effects in different region of phase space. At small values of  $x$ , for instance  $x < \sim 0.07$ , the nuclear structure function is less than nucleon structure function scaled by  $A$ . This is known as shadowing. As  $x$  grows bigger, nuclear structure functions get bigger than the free nucleon structure function. This is known as anti-shadowing. As  $x$  further increases, nuclear structure functions become less than the free nucleon ones again which is known as the EMC effect. In this section, we will concentrate on shadowing and anti-shadowing regions since those are the kinematic regions where the prompt photon production takes place. We refer the reader to [15] for a recent review of nuclear shadowing.

An intuitive explanation of nuclear shadowing and anti-shadowing effects in DIS depends on the reference frame of the nucleus. Of course, the physical observables such as structure functions can not depend on our choice of reference frame. However, working in different frames helps one identify the different physical mechanisms involved. In the rest frame of the nucleus and in perturbative QCD, shadowing of nuclear structure functions in DIS is due to multiple interaction of the  $q\bar{q}$  component of the photon wave function (emitted by the electron) with the nucleus. The amplitude of  $q\bar{q}A$  interaction is mostly imaginary at small  $x$  and multiple interactions of the pair with the nucleus introduces a phase difference between different amplitudes which leads to a destructive interference. This in turn reduces the nuclear cross section. In a non-perturbative description of shadowing, the photon is resolved in terms of its hadronic fluctuations which in turn multiply interact with the nucleus. The multiple interactions again reduce the nuclear cross sections due to destructive interference. In this frame, anti-shadowing at larger  $x$  is due to a large real part of the interaction amplitudes which interfere constructively with the imaginary part and lead to an enhancement of the nuclear cross section (structure functions).

In the infinite momentum frame where the nucleus is moving very fast, shadowing is caused by high parton density effects small  $x$ . The small  $x$  partons have a large longitudinal wavelength and can spatially overlap and recombine. These recombination effects reduce the nuclear parton number densities and hence the nuclear cross sections. Working in this frame enables one to treat nuclear shadowing and parton saturation in nucleons on the same footing due to the identical physical mechanism involved in both. Anti-shadowing is due to longitudinal momentum conservation (momentum sum rule) in this frame.

Even though there has been considerable amount of theoretical work done on nuclear shadowing and impressive progress made in understanding the physical principles of nuclear shadowing [15], we are far from having a precise and quantitative description of nuclear shadowing. In practice, one measures the nuclear structure functions in deep inelastic scattering of leptons on nuclei [16]. The measured structure functions are then used in nuclear collisions. The scale dependence of the nuclear structure functions is even less understood due to the limited range of  $Q^2$  covered in fixed target experiments. Also, shadowing of gluons is not well understood due to the fact that they can not be directly measured in DIS experiments. The working assumption is that high parton density effects are negligible and DGLAP evolution equations are valid in which case the gluon distribution function can be obtained from the scaling violation of the  $F_2$  structure functions. This assumption, however, will break down at small values of  $x$  due to high parton density effects [17] and one will need to measure the gluon distribution function differently.

In this work we will use two different parameterizations of nuclear structure functions due to Benesh, Qiu, Vary [18] and Eskola et al. [19]. Both parameterizations fit the current experimental data quite well even though they are somewhat different. Also, since there are no experimental data at the small  $x$ , high  $Q^2$  ( $Q^2 > 1\text{GeV}^2$ ) region, any parameterization of nuclear structure functions in this region is subject to large uncertainties. This is somewhat important for RHIC but becomes crucial for LHC. An  $eA$  collider such as the proposed eRHIC is urgently needed and would greatly improve our knowledge of nuclear structure functions in the small  $x$ , high  $Q^2$  region as well as reducing the theoretical uncertainties in the larger  $x$  region.

The parametrization of the nuclear shadowing function proposed by Benesh, Qiu and Vary is given by [18]

$$S(x, A) = \left\{ \begin{array}{ll} \alpha_3 - \alpha_4 x & x_0 < x \leq 0.6 \\ (\alpha_3 - \alpha_4 x_0) \frac{1+k_q \alpha_2 (1/x-1/x_0)}{1+k_q A^{\alpha_1} (1/x-1/x_0)} & x \leq x_0 \end{array} \right\} \quad (6)$$

It gives a good description of all EMC, NMC and E665 data [16]. The parameters  $k_q$ ,  $\alpha_1$ ,  $\alpha_2$ ,  $\alpha_3$  and  $x_0$  are fitted to deep inelastic data for the ratio  $F_2^A(x, Q^2)/F_2^D(x, Q^2)$  and can be found in [18]. In this parametrization, nuclear structure functions are independent of  $Q^2$  and shadowing of gluons is assumed to be the same as quarks. A more recent parameterization of the nuclear structure function is that of Eskola et al. [19] that also fits the existing experimental data quite well, has  $Q^2$  dependence and distinguishes between quark and gluon structure functions [19]. We show the nuclear shadowing ratio defined as  $S \equiv F_2^A/AF_2^N$  in Figure (2) using the parameterizations of BQV [18] and EKS [19]. Clearly, the two are quite different although both fit the experimental data fairly well. This signifies the need for a high energy collider experiment such as eRHIC to improve on the current measurements of the nuclear structure functions.

In this work, we will use both parameterizations and investigate the dependence of prompt photon production cross sections on our choice of nuclear structure functions.

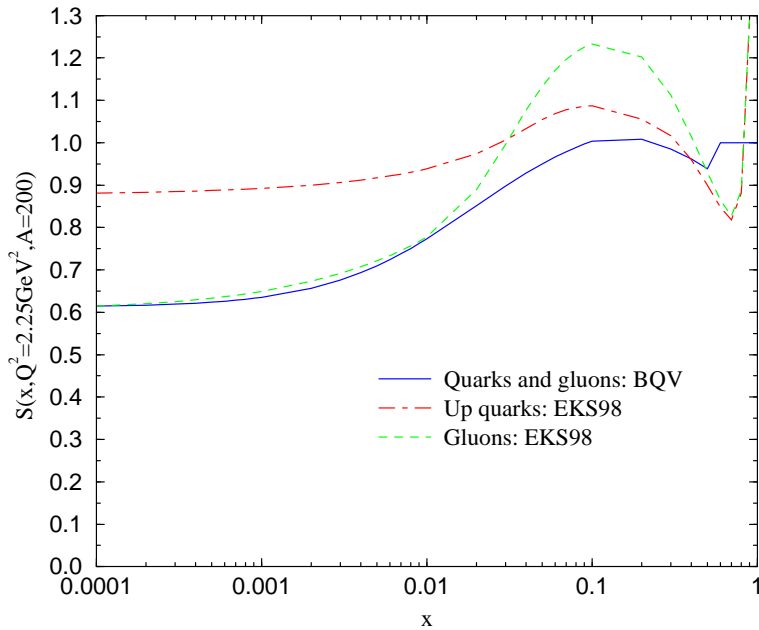


Figure 2: The nuclear shadowing ratio as parameterized by BQV [18] and EKS98 [19]).

### 3.2 Medium induced parton energy loss effects

Another difference between hadronic and heavy ion collisions is in the multiplicity of the final state particles produced. In high energy heavy ion collisions and in central rapidities, the multiplicity of particles produced per unit rapidity is much larger than that in hadronic collisions. Therefore, many body effects such as secondary collisions, which are negligible in hadronic collisions become important in high energy heavy ion collisions. Another example is the medium induced energy loss. In hadronic collisions, since the number density of particles per rapidity produced is small, one can neglect the multiple interactions of the produced partons with each other. On the other hand, in high energy heavy ion collisions, due to high multiplicities per unit rapidity, the multiple interactions of produced partons with each other can not be neglected. As a consequence of multiple interactions with the medium, produced particles can lose energy before hadronizing. This affects their energy and momentum spectrum. Energy loss of energetic partons passing through a dense medium has been a hot topic lately [20]. There has been a considerable progress made in understanding the different forms of the energy loss in different limits. It has been shown, for a finite size medium, that parton energy loss increases with increasing parton energy [20]. Current calculations of energy loss effects are done at the leading order  $O(\alpha_s)$  and a next-to-leading order calculation is not presently available.

A rigorous treatment of energy loss effects in a heavy ion collision is extremely complicated and beyond the scope of this work. Rather, we will take a phenomenological approach to medium induced energy loss in nuclear collisions and use a model of Wang, Huang and Sarcevic [21], to estimate energy loss effects in high energy heavy ion collisions.

In this commonly used model, it is assumed that the main effect of multiple interactions in the medium can be accommodated by modifying the photon fragmentation functions. In the central rapidity region, parton produced in the hard collision is traversing the nuclear medium and losing its energy as a result of multiple interactions with the deconfined medium. This parton will hadronize outside the nuclear medium but with a reduced energy.

In the energy loss model of Wang, Huang and Sarcevic [21], the parton to photon fragmentation function,  $zD_{a/\gamma}^0(z, Q_f^2)$ , which gives the probability for a parton to fragment into a photon, is modified to include multiple scatterings of the fragmenting parton from the nuclear medium before it fragments. The nuclear fragmentation function  $zD_{a/\gamma}(z, Q_f^2)$  is given in terms of the photon fragmentation function  $zD_{a/\gamma}^0(z, Q_f^2)$  by [21]

$$zD_{a/\gamma}(z, \Delta L, Q_f^2) = \frac{1}{C_N^a} \sum_{n=0}^N P_a(n) \left[ z_n^a D_{a/\gamma}^0(z_n^a, Q_f^2) + \sum_{j=1}^n \bar{z}_a^j D_{g/\gamma}^0(\bar{z}_a^j, Q_f^2) \right] \quad (7)$$

where  $z_n^a = z/(1 - (\sum_{i=0}^n \epsilon_i^a)/E_t)$ ,  $\bar{z}_a^j = zE_t/\epsilon_a^j$  and  $P_a(n)$  is the probability that a parton of flavor  $a$  traveling a distance  $\Delta L$  in the nuclear medium will scatter  $n$  times. It is given by

$$P_a(n) = \frac{(\Delta L/\lambda_a)^n}{n!} e^{-\Delta L/\lambda_a}, \quad (8)$$

and  $C_N^a = \sum_{n=0}^N P_a(n)$ .

The first term in Eq. (7) corresponds to the fragmentation of the leading parton  $a$  with reduced energy  $E_t - \sum_{i=0}^n \epsilon_i^a$  after  $n$  gluon emissions and the second term comes from the  $j$ -th emitted gluon having energy  $\epsilon_a^j$ , where  $\epsilon_a^j$  is the energy loss of the parton  $a$  after  $j$ -th scattering. Since we are studying the energy loss effects only phenomenologically, we will consider two different cases for the energy loss per collision,  $\epsilon_a^j$ . First we will take it to be constant, as considered for example, in [22]. We will also consider energy dependent energy loss in the form of  $\epsilon_a^j = \alpha_s \sqrt{\mu^2 \lambda_a} E_a^j$ , where  $E_a^j$  is the energy of the parton  $a$  after  $j$  scatterings,  $\lambda_a$  is the inelastic mean free path of parton  $a$  and  $\mu^2$  represent a screening mass generated by the plasma and serves as an infrared cut off. It should be emphasized that the general form of the energy loss per scattering,  $\epsilon_a^j$ , is theoretically unknown and we consider two possible cases. In order to study theoretical uncertainties involved, we will take several values for the constant energy loss and in the case of energy-dependent energy loss we will vary parameters  $\mu^2$  and  $\lambda_a$ .

The nuclear fragmentation functions of quarks and gluons as defined in (7), with energy dependent energy loss, are shown in Figure (3). Here we have taken  $\mu^2 = 1\text{GeV}^2$  and  $\lambda_a = 1\text{fm}$ . The constant energy loss case is quite similar. For the photon fragmentation function,  $zD_{a/\gamma}^0(z, Q_f^2)$ , we use the parameterization of [10]. The parton to photon fragmentation functions in a nuclear medium are enhanced at small  $z$  and suppressed at large  $z$  as compared to the fragmentation functions in vacuum. This is due to the fact that high energy (high  $z$ ) partons multiply scatter from the medium and lose their energy which shifts their energy fraction  $z$  to a smaller value. The nuclear fragmentation function

obtained assuming constant energy loss per scattering has qualitatively the same behavior as a function of  $z$ .

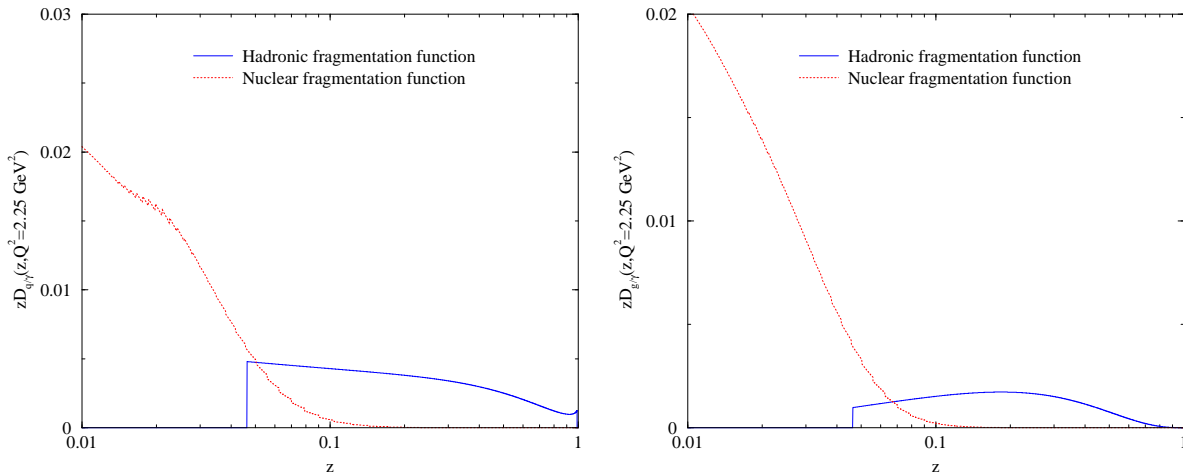


Figure 3: The photon fragmentation function, a)  $zD_{q/\gamma}^0(z, Q_f^2)$  (solid line) [10] and the nuclear fragmentation function  $zD_{q/\gamma}(z, Q_f^2)$  obtained using (7) (dashed line) and b)  $zD_{g/\gamma}^0(z, Q_f^2)$  (solid line) [10] and the corresponding nuclear fragmentation function  $zD_{g/\gamma}(z, Q_f^2)$  (dashed line).

As one goes to higher energies in heavy ion collisions, one probes smaller and smaller energy fractions  $z$  in the fragmentation functions. The fragmentation functions,  $zD_{q/\gamma}^0(z, Q_f^2)$ , are fit to the experimental data and parameterized. However, the existing data does not cover the  $z$  ranges which will be explored by LHC. Therefore, the current parameterizations of parton to photon fragmentation functions are set equal to zero below some energy fraction,  $z < z_0 \sim 0.01$ . This is shown in Figure (3). In the kinematic region appropriate to LHC, however, one will need to know the fragmentation functions below this energy fraction. Therefore, we use both the standard (hadronic) fragmentation functions which are zero below  $z_0$  and another parameterization which is identical to the standard one for  $z > z_0$  but is set equal to a constant for  $z < z_0$ , i.e.  $zD_{q,g/\gamma}^0(z, Q_f^2) = zD_{q,g/\gamma}^0(z = z_0, Q_f^2)$  for  $z \leq z_0$ . We have checked that the difference between the two parameterizations leads to a negligible ( $< 1\%$ ) difference in the nuclear cross section. The reason is that the average  $z$  is sufficiently large ( $z \sim 0.1$ ) and thus the results are not sensitive to the variation of fragmentation functions in the small  $z$  region. Also, partonic cross sections at small  $z$  are power suppressed and do not contribute significantly.

The parton mean free path  $\lambda_a$  and the screening mass  $\mu^2$  are largely unknown and in principle depend on the parton species and the medium temperature. In this work, we treat  $\mu^2$  and  $\lambda_a$  as unknown parameters and show the dependence of our results on a physically reasonable variation of them in Figure (4). By varying these parameters,  $\mu^2$  and  $\lambda_a$ , we study theoretical uncertainties. Experimental determination of these parameters would be difficult. Energy dependent form of energy loss,  $\epsilon_a^j = \alpha_s \sqrt{\mu^2 \lambda_a E_a^j}$ , is, strictly speaking, valid only for coherent photon radiation. Here, we have considered this form just

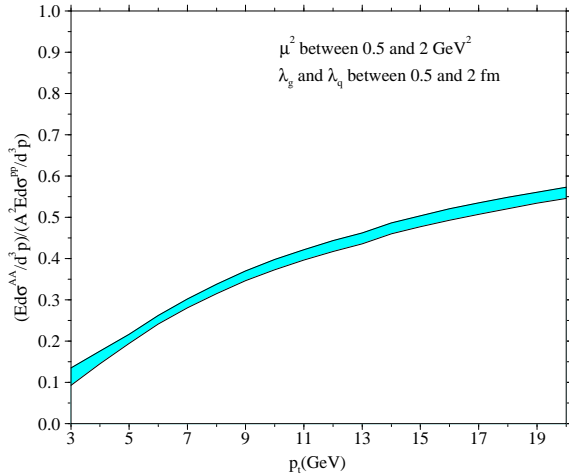


Figure 4: The uncertainty in prompt photon cross section at  $\sqrt{s} = 5.5$  TeV due to variation of energy-dependent energy loss parameters.

as a phenomenological expression that gives photon  $p_t$  distribution that we could compare with the constant energy loss case. The precise form of energy loss in a realistic nuclear collision, such as those at RHIC and LHC energies, is not well understood at the moment and is expected to be extremely complicated.

## 4 Discussion

We show our results for the prompt photon cross section in nuclear collisions at LHC energies in Figures (5), (6) and (7). We use different forms of nuclear shadowing and energy-dependent energy loss with  $\mu^2 = 1\text{GeV}^2$  and  $\lambda_a = 1\text{fm}$  (Figures 5 and 6) or a constant energy loss (Figure 7). We find nuclear effects at LHC to be strikingly large. The nuclear cross sections can be reduced by 90% at  $p_t = 3$  GeV and 50% at  $p_t = 20$  GeV for the energy dependent energy loss scenario. The constant energy loss of 2 GeV per scattering leads to the similar size effects while smaller energy losses per scattering, such as 1 GeV, 0.5 GeV and 0.25 GeV lead to smaller suppression of the nuclear cross section. In Figure (5) BQV parameterization of shadowing is used which is  $Q^2$  independent. This reflects itself in almost constant ( $\sim 30\%$ ) contribution of shadowing to the suppression of the nuclear cross section at all  $p_t$ . On the other hand, energy loss effects become smaller at larger  $p_t$ 's ( $\sim 50\%$  at  $p_t = 3$  GeV and  $\sim 20\%$  at  $p_t = 20$  GeV).

In Figure (6) we use both the BQV [18] and the EKS98 [19] parameterization of shadowing. The EKS98 parameterization has  $Q^2$  dependence and distinguishes between quark and gluon shadowing while the BQV parameterization is  $Q^2$  independent and does not distinguish between quark and gluon shadowing. The difference at low  $p_t$  ( $p_t \sim 3$  GeV) is small, about 4% while at  $p_t = 20$  GeV it is about 20%. This is mainly due to the  $Q^2$

dependence of EKS98 parameterization.

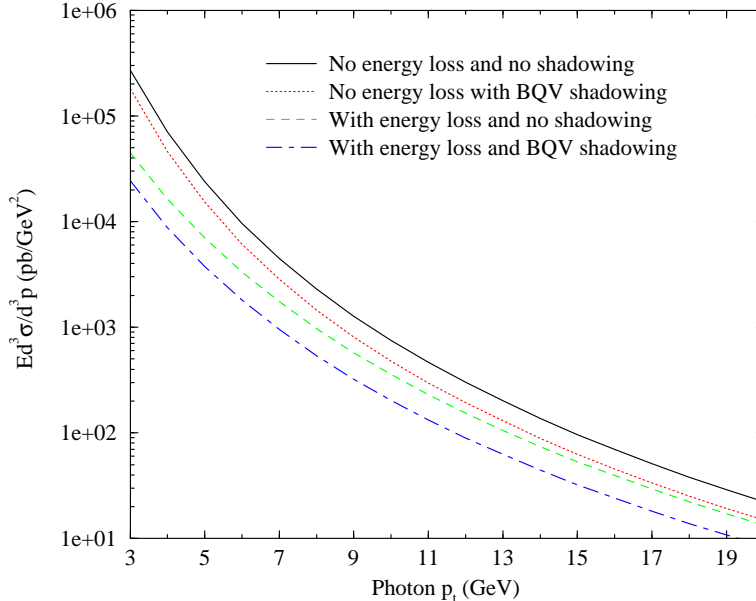


Figure 5: Prompt photon cross section in the central rapidity region at  $\sqrt{s} = 5.5$  TeV without nuclear effects (solid line), with BQV [18] shadowing and no parton energy loss (dotted line), with parton energy loss and no shadowing (dashed line) and with BQV [18] shadowing and parton energy loss (dashed-dotted line). Parton energy loss is taken to be energy dependent,  $\epsilon_a^j = \alpha_s \sqrt{\mu^2 \lambda_a E_a^j}$ , with  $\mu^2 = 1\text{GeV}^2$  and  $\lambda_a = 1\text{fm}$ .

In Figure (7) we show the dependence of the photon cross section on the form of energy loss used, by considering different values of the constant energy loss. For comparison, we also show the energy-dependent energy loss case with  $\mu^2 = 1\text{GeV}^2$  and  $\lambda_g = \lambda_q = 1\text{fm}$ . It is clear that the magnitude of the nuclear cross section is sensitive to the magnitude of the energy loss.

To illustrate the importance of doing the full next-to-leading order calculation of prompt photon production at the LHC, we show the nuclear  $K$ -factors, defined as the ratio of  $NLO/LO$  and as the ratio of  $NLO/(LO + Brems.)$  cross sections in Figure (8). It should be clear that the higher order corrections (beyond NLO) are important at low  $p_t$  and that our analysis is only qualitatively reliable there. The dependence of cross section on the choice of renormalization, factorization and fragmentation scales is shown in Figure (9). Varying scales from  $0.5p_t$  to  $2.0p_t$  results in theoretical uncertainty of about 30%. This indicates the importance of including higher order terms, as does the large  $K$  factor values presented in Figure (8). We refer the reader to [11] for a complete analysis of scale dependence of prompt photon cross section in  $pp$  collisions.

We find that nuclear effects at LHC are significant and should be easily detectable. Nuclear shadowing effects are large and need to be better understood. In Figure (10) we show the rescaled nuclear cross section using the BQV and EKS98 nuclear shadowing. The

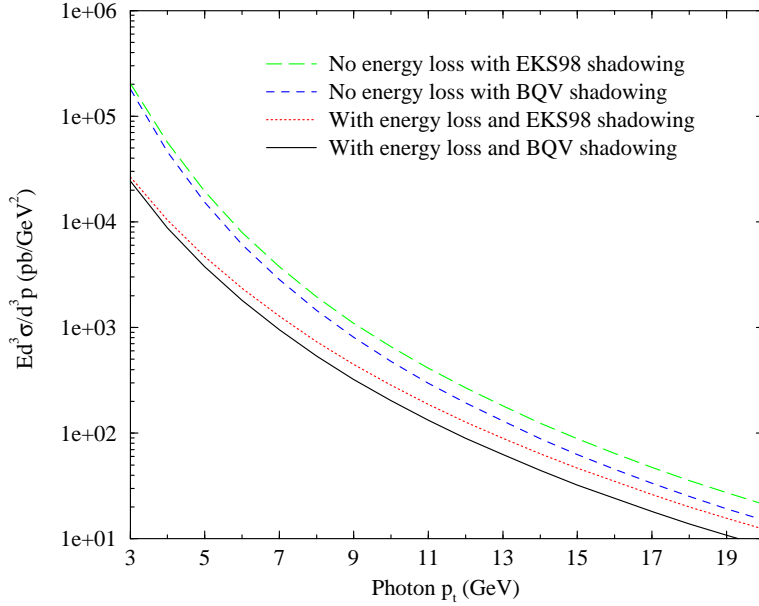


Figure 6: Prompt photon cross section in the central rapidity region at  $\sqrt{s} = 5.5$  TeV obtained with EKS98 [19] shadowing and without parton energy loss (dotted line), with parton energy loss (dashed line), with BQV shadowing [18] and no parton energy loss (solid line) and with energy loss (dot-dashed line). Parton energy loss is taken to be energy dependent,  $\epsilon_a^j = \alpha_s \sqrt{\mu^2 \lambda_a E_a^j}$ , with  $\mu^2 = 1\text{GeV}^2$  and  $\lambda_a = 1\text{fm}$ .

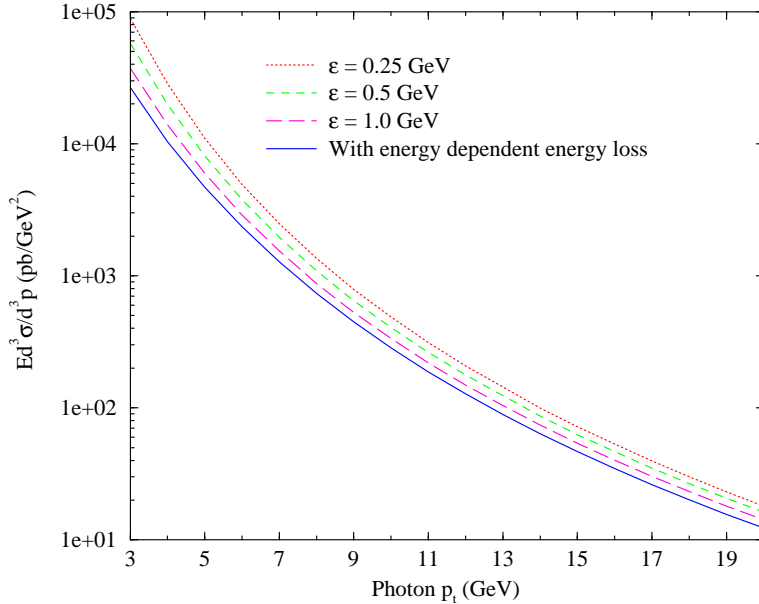


Figure 7: Prompt photon cross section in the central rapidity region at  $\sqrt{s} = 5.5$  TeV obtained with EKS98 shadowing [19] and with different values for parton energy loss .

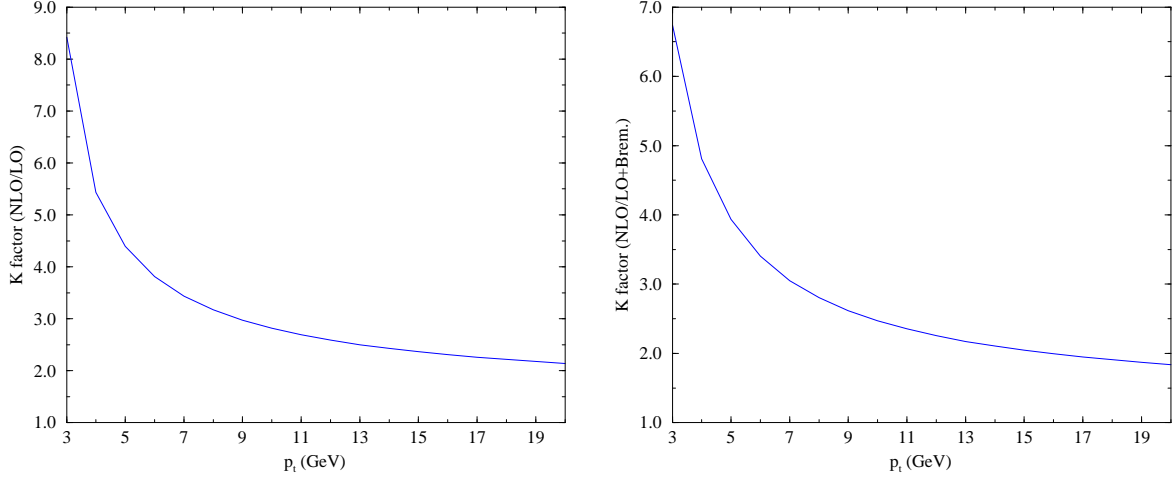


Figure 8: a) The nuclear K-factor defined as the ratio of NLO prompt photon cross section in heavy-ion collisions,  $E \frac{d\sigma}{d^3p}$ , to the LO cross section and b) the K-factor defined as the ratio of NLO to the LO plus bremsstrahlung cross sections. Parton energy loss is taken to be energy dependent,  $e_a^j = \alpha_s \sqrt{\mu^2 \lambda_a E_a^j}$ , with  $\mu^2 = 1\text{GeV}^2$  and  $\lambda_a = 1\text{fm}$ .

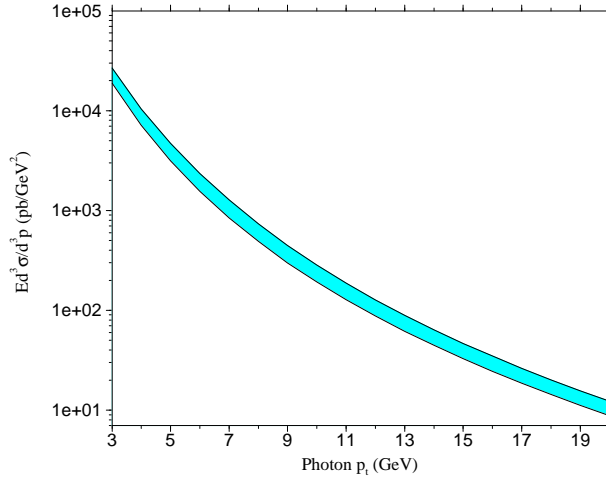


Figure 9: The uncertainty of the photon cross section due to varying factorization, renormalization and fragmentation scales ( $Q = M = Q_F$ ) between  $0.5p_t$  and  $2p_t$ . Parton energy loss is taken to be energy dependent, with  $\mu^2 = 1\text{GeV}^2$  and  $\lambda_a = 1\text{fm}$ .

difference between the two parameterizations of nuclear shadowing is significant at large  $p_t$ . This raises the possibility that one could study the  $Q^2$  dependence of nuclear shadowing by measuring the  $p_t$  spectrum of prompt photons since this difference is independent of the form of the energy loss per scattering used.

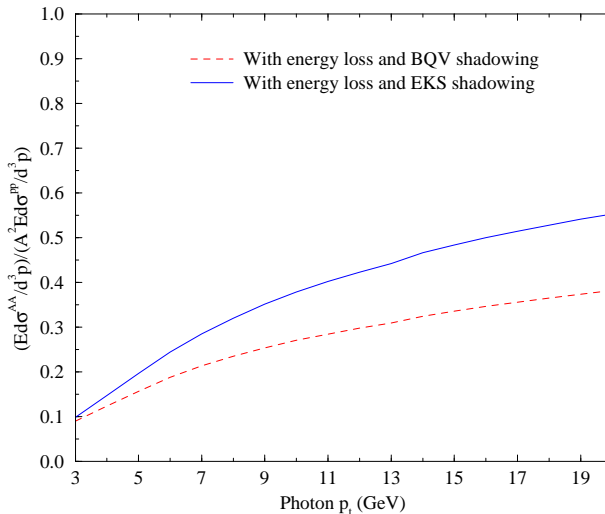


Figure 10: The rescaled prompt photon cross section in the central rapidity region at  $\sqrt{s} = 5.5$  TeV using BQV [18] and EKS98 [19] shadowing and energy-dependent energy loss with  $\mu^2 = 1\text{GeV}^2$  and  $\lambda_a = 1\text{fm}$ .

Current parameterizations of nuclear shadowing in the kinematic region appropriate to LHC energies are extrapolations from low energy fixed target data and subject to large uncertainties. A precise quantitative knowledge of the nuclear structure functions at the small  $x$ , large  $Q^2$  kinematic region is crucial. A lepton-nucleus collider such as eRHIC is urgently needed.

Energy loss effects are also large. In Figure (11) we show the rescaled nuclear cross section for the case of constant energy loss. Whether one can distinguish experimentally between different energy loss scenarios will depend on our precise knowledge of nuclear structure functions and also on the precision of the prompt photon measurements at RHIC and LHC. Distinguishing prompt photons from those coming from decays of pions and eta's is notoriously difficult. Also, one expects that the calculation of the ratio of prompt photons to pions would reduce some of theoretical uncertainties such as scale dependence and intrinsic  $k_t$  effects, thus making the NLO calculation even more reliable [23]. We intend to calculate this ratio in the near future [24].

## Acknowledgments

We would like to thank P. Aurenche and M. Werlen for providing us with the fortran routines for calculating double differential distributions for photon production in hadronic collisions and for many useful discussions. J. J-M would like to thank S. Jeon, M. Tannenbaum and X-N. Wang for many helpful discussions. J. J-M is grateful to LBNL nuclear

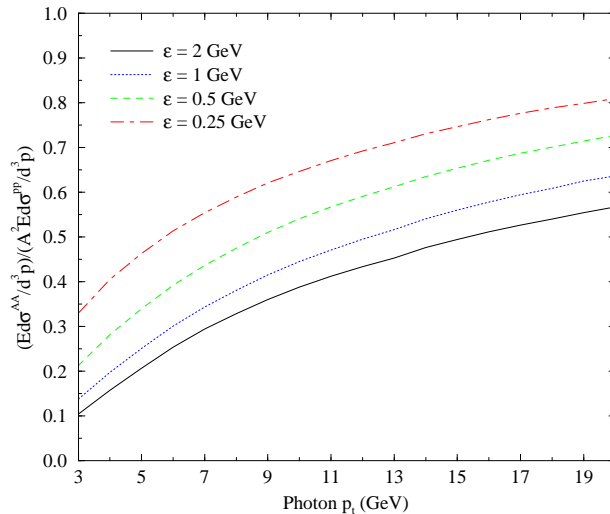


Figure 11: The rescaled prompt photon cross section in the central rapidity region at  $\sqrt{s} = 5.5$  TeV obtained using constant energy loss and EKS98 [19] nuclear shadowing form.

theory group for the use of their computing resources. This work was supported in part through U.S. Department of Energy Grants Nos. DE-FG03-93ER40792 and DE-FG02-95ER40906.

## References

- [1] See for example, the proceedings of the XIVth International Conference on Ultrarelativistic Nucleus-Nucleus Collisions (Quark Matter 1999), *Nucl. Phys.* **A661** (1999).
- [2] L. McLerran and T. Toimela, *Phys. Rev.* **D31**, 545 (1985); E.V. Shuryak, *Phys. Lett.* **B78**, 150 (1978); *Phys. Rep.* **61**, 72 (1980).
- [3] J. Kapusta, P. Lichard and D. Seibert, *Phys. Rev.* **D44**, 2774 (1991); Erratum: *ibid.* **D47**, 4171 (1993).
- [4] N. Hammon, A. Dumitru, H. Stocker and W. Greiner, *Phys. Rev.* **C57**, 3292 (1998); A. Dumitru and N. Hammon, hep-ph/9807260.
- [5] D.K. Srivastava, nucl-th/9911047; D.K. Srivastava and B. Sinha, nucl-th/0006018.
- [6] J. Jalilian-Marian, K. Orginos and I. Sarcevic, *Phys. Rev.* **C63**, 041901 (2001).
- [7] P. Aurenche, R. Baier, M. Fontannaz and D. Schiff, *Nucl. Phys.* **B297**, 661 (1988).
- [8] P. Aurenche, P. Chiappetta, M. Fontannaz, J. Guillet and E. Pilon, *Nucl. Phys.* **B399**, 34 (1993).
- [9] A.D. Martin, R.G. Roberts, W.J. Stirling and R.S. Thorne, *Eur. Phys. J.* **C14**, 133 (2000).
- [10] M. Gluck, E. Reya and A. Vogt, *Phys. Rev.* **D48**, 116 (1993); Erratum: *ibid.* **D51**, 1427 (1995); L. Bourhis, M. Fontannaz and J.Ph. Guillet, *Eur. Phys. J.* **C2**, 529 (1998).
- [11] P. Aurenche, M. Fontannaz, J.Ph. Guillet, B. Kniehl, E. Pilon and M. Werlen, *Eur. Phys. J.* **C9**, 107 (1999).

- [12] G. Sterman and W. Vogelsang, hep-ph/0011289 and references therein.
- [13] J. Houston, E. Kovacs, S. Kuhlmann, H. Lai, J. Owens and W. Tung, *Phys. Rev.* **D51**, 6139 (1995); L. Apanasevich et al., *Phys. Rev.* **D59**, 074007 (1999); *ibid.* **D63**, 014009 (2001).
- [14] Report of the working group on photon and weak boson production, hep-ph/0005226.
- [15] M. Arneodo, *Phys. Rep.* **240**, 301 (1994).
- [16] M.R. Adams, et al., *Phys. Rev. Lett.* **68**, 3266 (1992).
- [17] L. McLerran and R. Venugopalan, *Phys. Rev.* **D49**, 335 (1994); **D49**, 2233 (1994); J. Jalilian-Marian, A. Kovner, A. Leonidov and H. Weigert, *Phys. Rev.* **D59**, 034007 (1999); *ibid.* **D59**, 014015 (1999); J. Jalilian-Marian and X-N. Wang, *Phys. Rev.* **D60**, 054016 (1999); hep-ph/0005071; Z. Huang, H.J. Lu and I. Sarcevic, *Nucl. Phys.* **A637**, 70 (1998).
- [18] C.J. Benesh, J. Qiu and J.P. Vary, *Phys. Rev.* **C123**, 1015 (1994).
- [19] K. Eskola, V. Kolhinen and P. Ruuskanen, *Nucl. Phys.* **B535**, 351 (1998); K. Eskola, V. Kolhinen and C. Salgado, *Eur. Phys. J.* **C9**, 61 (1999).
- [20] R. Baier, Y. Dokshitzer, A. Mueller, S. Peigne and D. Schiff, *Nucl. Phys.* **B483**, 291 (1997); *ibid.* **B484**, 265 (1997); R. Baier, D. Schiff and B.G. Zakharov, hep-ph/0002198.
- [21] X-N. Wang, Z. Huang and I. Sarcevic, *Phys. Rev. Lett.* **77**, 231 (1996); X-N. Wang and Z. Huang, *Phys. Rev.* **C55** 3047 (1997).
- [22] X-N. Wang, *Phys. Rev.* **C58**, 2321 (1998), **C61**, 064910 (2000).
- [23] M. Tannenbaum, private communication.
- [24] J. Jalilian-Marian, S. Jeon, K. Orginos and I. Sarcevic, in preparation.

